Computer Modeling in Engineering & Sciences
DOI:10.32604/cmes.2020.010304
Article

Tech Science Press

Effect of Absorption of Patch Antenna Signals on Increasing the Head Temperature

Mohamed Abbas[1,3,*], Ali Algahtani[2,6], Amir Kessentini[2,4,7], Hassen Loukil[1,5], Muneer Parayangat[1], Thafasal Ijyas[1] and Abdul Wase Mohammed[1]

[1]Electrical Engineering Department, College of Engineering, King Khalid University, Abha, 61421, Saudi Arabia
[2]Department of Mechanical Engineering, College of Engineering, King Khalid University, Abha, 61421, Saudi Arabia
[3]Department of Computers and Communications, College of Engineering, Delta University for Science and Technology, Gamasa, 35712, Egypt
[4]Laboratory of Electromechanical Systems (LASEM), National Engineering School of Sfax, University of Sfax, Sfax, 3038, Tunisia
[5]Electronics and Information Technology Laboratory, University of Sfax, National Engineering School of Sfax, Sfax, 3038, Tunisia
[6]Research Center for Advanced Materials Science, King Khalid University, Abha, 61413, Saudi Arabia
[7]Nabeul's Foundation Institute for Engineering Studies, University of Carthage, IPEIN, Nabeul, 8000, Tunisia
*Corresponding Author: Mohamed Abbas. Email: mabas@kku.edu.sa
Received: 25 February 2020; Accepted: 01 April 2020

Abstract: Every new generation of antennas is characterized by increased accuracy and faster transmission speeds. However, patch antennas have been known to damage human health. This type of antenna sends out electromagnetic waves that increase the temperature of the human head and prevent nerve strands from functioning properly. This paper examines the effect of the communication between the patch antenna and the brain on the head's temperature by developing a hypothetical multi-input model that achieves more accurate results. These inputs are an individual's blood and tissue, and the emission power of the antenna. These forces depend on the permeability and conductivity characteristics of the metal from which the antenna is fabricated. The proposed model is the first one that links the material the antenna is manufactured from and the head's temperature. The results show that there are only a small number of materials that should be used as antenna covers. These materials are in the form of thin films. By using these thin films at different temperatures, the risk to the head can be reduced. This paper finds that the best results were obtained when the patch antenna was made of one of the following materials operating at a specific temperature: traditional materials at 305°K; casting cast steel at around 295°K; bismuth telluride (Bi2Te3) at 290°K; or barium sodium niobate at 310°K.

Keywords: Brain; patch antenna; head overheating; waves behavior; materials properties

1 Introduction

Different techniques used in the field of wireless communications pose a number of health risks to people. For instance, some smartphones now incorporate patch antennas, which send out electromagnetic waves that can be very dangerous to the human brain, as they can overheat the head. The following

illustrates the behavior of these waves. Head overheating causes hazardous intra-mind warmth storing up and exceptional de-compensation of physiological limits [1]. High temperatures can prevent nerve strands from working normally, meaning that messages may not be able get to and from the brain. When this happens, an individual may experience fatigue, weakness, or problems with balance or vision. People may need to lower their head temperature while using these types of antennas. Therefore, this research aims to develop a model of a hypothetical communication process between the antenna and the brain. A key factor in this proposal is the antenna material [2].

The research suggests the type of material suitable for manufacturing antenna and comparing the effect of this material with currently used materials. The numerical investigation of Explicit Ingestion Rate and temperature conveyance inside a genuine kid head model is presented to cell phone radiation. The specific absorption rate (SAR) and temperature dissemination are acquired by numerical arrangements of the condition of electromagnetic waves proliferation and by the condition of bioheat, individually, and appear inside tissues and organs during the emission of electromagnetic radiation from a cell phone. The impact of expanding the distance from a mobile phone to an individual's head is resolved because of the warmth produced by radiofrequency waves [1,2]. Mix the hyperthermia implement framework is intended for the head and neck region taking a shot at recurrence 434 MHz with UWB radar reception apparatus cluster for differential temperature location [3]. A calculation is proposed to give conveyances at different frequencies utilizing a solitary reproduction. The head tissue parameters are utilized from the accessible three-term Debye coefficients got by the exploratory information from 500 MHz to 20 GHz [4].

A 28-GHz shaft-directing patch exhibiting a dipole receiving wire is utilized, and plane waves are used to research the temperature in a multi-layer model of the human head and its connection with control thickness measurements [5]. The theory that skin temperature, particularly of the head, is fit for balancing the warmth generated by exercise when exposed to harsh elements [6]. A trial framework was created to analyze a scientific re-creation of the bloodstream in a human head by utilizing a strong mind model built utilizing silicon elastic in the state of a cerebrum dependent on X-ray information, considering the metabolic warmth emitted by three film radiators and including six sensors for the estimation of provincial mind temperature [7]. Another numerical plan dependent on the TLM strategy is applied for figuring warm dissemination in a human head presented to plane wave at 900 MHz [8]. The present research examinesthe connection between the maximal rise in temperature in various models of the human head, for frequencies from 1 GHz to 10 GHz. A half-wave dipole radio wire is considered as a wave source at different frequencies [9]. It is discovered that the highest SARs are 0.823 W/kg and 1.187 W/kg for frequencies of 900 MHz and 1800 MHz, respectively. The SAR values obtained from this investigation are well below other cases [10]. Examinations of the relative impact of a hydrophilic gathering on Krafft temperature, surface exercises, and rheological practices of critical amidobetaines with sulfonate, hydroxyl-sulfonate, or carboxylate were analyzed in [11].

The electromagnetic impact of head-implantable transmitting gadgets based on ultra wideband (UWB) radio technology are introduced. Models are built around an implantable UWB radio wire tuned to work at 4 GHz with a 10-dB transfer speed of around 1 GHz when it is placed in a model of a human head [12]. The sub-atomic portrayal of two about isogenic lines with differentiating head-shaping limit was researched. Head-shaping limit was better for heat-tolerant (HT) than heat-delicate (HS) broccoli under warmth stress [13]. An examination is directed in an anechoic chamber with a normal of 45 minutes talking hour with two distinct sorts of cell phone, interior and outside reception apparatus serving diverse radio recurrence go, 900 MHz and 1800 MHz [14]. The aim of this research is to reduce the head's temperature when using smartphones that contain patch antennas. This is to be achieved by developing a proposed model for a hypothetical communication process between the anaerobic and the brain. This model is characterized by its ability to bind the type of material manufactured aerobic to a number of biological and technological factors that affect the temperature of the head. The model then offers a method for

selecting the best material for making the antenna in order to reduce the head's temperature when the electromagnetic waves from this contact are emitted.

2 Proposed Paradigm for Virtual Contact between the Brain and the Patch Antenna

In this section, a model for a hypothetical communication process is presented. By studying a number of biological and technological factors and linking these factors to total head temperature, the model not only examines the impact of the antenna on the brain but also on the surrounding tissue. Limited warmed tissue was considered. It was assumed that the blood stayed vasculature and everything encompassing the blood was tissue. Rationing vitality for a point in the tissue and blood is brought about by the emanated intensity of the fix receiving wire (P) that influences both blood and tissues by various qualities brought about the accompanying condition of convective vitality [15,16]:

$$\frac{\partial T_i}{\partial t} = \frac{1}{(\rho\psi)_i}[\nabla.\Gamma_i\nabla T_i + P_i] - \upsilon_i.\nabla T \tag{1}$$

where ρ is the density, ψ is the specified heat, Γ is the thermal conductivity, υ is the velocity, and i could refer to tissue or blood. Temperature T could be reached using the separation of variables method. Consider the power radiated from the patch P can be determined in spherical coordinates using Eq. (2), where ε represents electric permittivity and μ is the magnetic permeability of the removable thin film that covered the patch antenna, as shown in Fig. 1 [17].

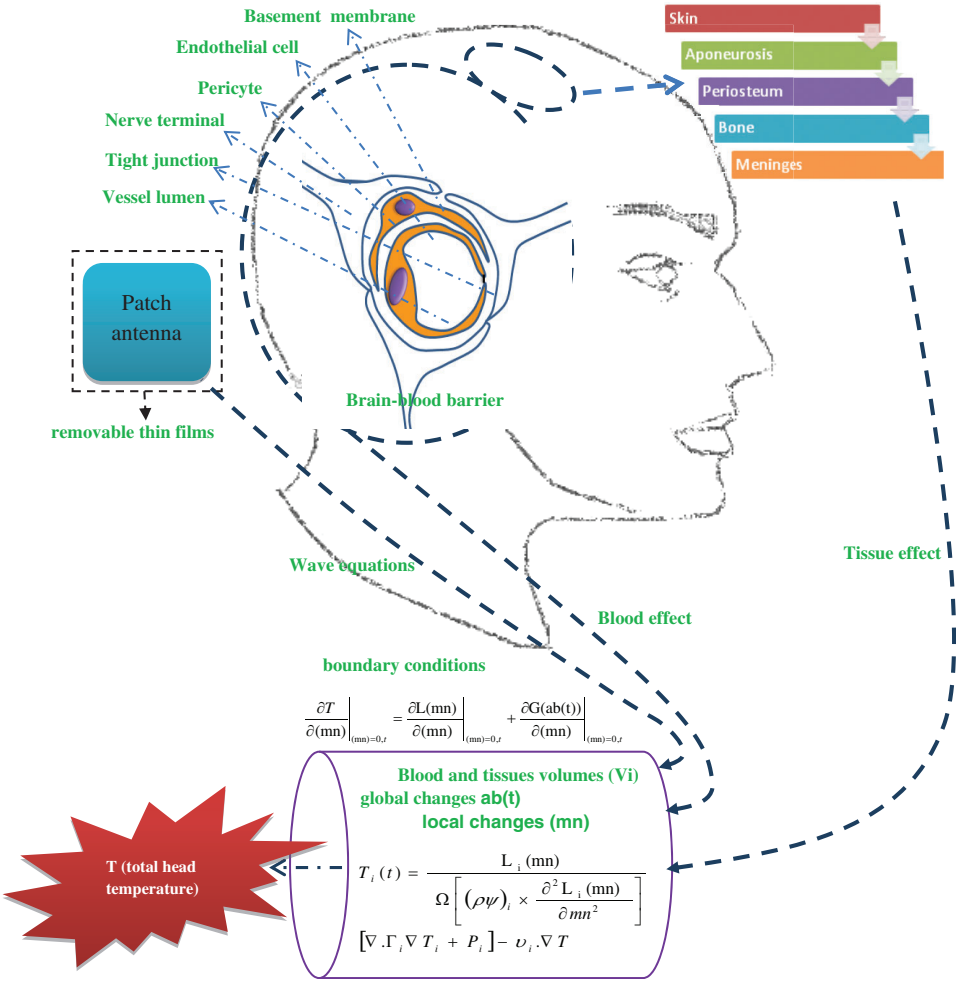

Figure 1: Proposed paradigm for measuring the effect of patch antenna-brain connectivity on head temperature

$$P = \frac{1}{2\sqrt{\frac{\mu}{\varepsilon}}} \int_0^{2\pi} \int_0^{2\pi} \left(|E_\theta|^2 + |E_\phi|^2 \right) (r^2)(\sin\theta) d\theta d\phi \tag{2}$$

Using Eqs. (1) and (2), the convective energy equation is as follows:

$$\frac{\partial T_i}{\partial t} = \frac{1}{(\rho\psi)_i} \left[\nabla.\Gamma_i \nabla T_i + \frac{1}{2\sqrt{\frac{\mu}{\varepsilon}}} \int_0^{2\pi} \int_0^{2\pi} \left(|E_\theta|^2 + |E_\phi|^2 \right) (r^2)(\sin\theta) d\theta d\phi_i \right] - \upsilon_i.\nabla T \tag{3}$$

From Eq. (3), it is clear that the power emitted by the antenna is directly proportional to the change in the temperature of tissue and blood in the brain. When the power emitted by the antenna increases, the change in tissue temperature also increases.

Working in the spherical coordinates, then the following equations are applied:

$$\nabla T_i = \frac{1}{r^2} \frac{\partial (r^2 T_{ir})}{\partial r} + \frac{1}{r(\sin\theta)} \frac{\partial}{\partial \theta} (T_i(\sin\theta)) + \frac{1}{r(\sin\theta)} \frac{\partial}{\partial \phi} T_i \phi \tag{4}$$

$$\nabla.\Gamma_i \nabla T_i = \frac{1}{r^2} \frac{\partial (r^2 \Gamma_i \nabla T_{ir})}{\partial r} + \frac{1}{r(\sin\theta)} \frac{\partial}{\partial \theta} (\Gamma_i \nabla T_i(\sin\theta)) + \frac{1}{r(\sin\theta)} \frac{\partial}{\partial \phi} \Gamma_i \nabla T_i \phi \tag{5}$$

Eqs. (4) and (5) can lead to Eq. (6):

$$\begin{aligned} \nabla.\Gamma_i \nabla T = & \frac{1}{r^2} \frac{\partial \left(r^2 \Gamma_i \left(\frac{1}{r^2} \frac{\partial (r^2 T_{ir})}{\partial r} + \frac{1}{r(\sin\theta)} \frac{\partial}{\partial \theta} (T_i(\sin\theta)) + \frac{1}{r(\sin\theta)} \frac{\partial}{\partial \phi} T_i \phi \right)_r \right)}{\partial r} \\ & + \frac{1}{r(\sin\theta)} \frac{\partial}{\partial \theta} \left(\Gamma_i \left(\frac{1}{r^2} \frac{\partial (r^2 T_{ir})}{\partial r} + \frac{1}{r(\sin\theta)} \frac{\partial}{\partial \theta} (T_i(\sin\theta)) + \frac{1}{r(\sin\theta)} \frac{\partial}{\partial \phi} T_i \phi \right) (\sin\theta) \right) \\ & + \frac{1}{r(\sin\theta)} \frac{\partial}{\partial \phi} \Gamma_i \left(\frac{1}{r^2} \frac{\partial (r^2 T_{ir})}{\partial r} + \frac{1}{r(\sin\theta)} \frac{\partial}{\partial \theta} (T_i(\sin\theta)) + \frac{1}{r(\sin\theta)} \frac{\partial}{\partial \phi} T_i \phi \right) \phi \end{aligned} \tag{6}$$

Now, consider L(mn) is the function of the local changes in metabolic neural activity (mn). G(ab) are the global changes caused by changing the temperature of arterial blood with time (ab(t)). This relationship is represented in Eq. (7):

$$\mathrm{T(mn, ab(t))} \;=\; \mathrm{L(mn)} \;\times\; \mathrm{G(ab(t))} \tag{7}$$

$$\frac{\partial T}{\partial t} = \frac{\partial [\mathrm{L(mn).G(ab(t))}]}{\partial t} = \mathrm{L(mn).} \frac{\partial [\mathrm{G(ab(t))}]}{\partial t} \tag{8}$$

Consider Ω is a species or thermal diffusion coefficient, then:

$$\Omega \frac{\partial^2 T}{\partial mn^2} = \Omega \frac{\partial^2 [\mathrm{L(mn).G(ab(t))}]}{\partial mn^2} = \Omega T(t) \frac{\partial^2 \mathrm{L(mn)}}{\partial mn^2} \tag{9}$$

Eq. (4) could be represented as follows:

$$\frac{\partial T}{\partial t} = \frac{\Omega T(t)}{\mathrm{L(mn)}} \frac{\partial^2 \mathrm{L(mn)}}{\partial mn^2} \tag{10}$$

By merging Eqs. (1) and (5), the following equation emerges:

$$\frac{\Omega T_i(t)}{\mathrm{L_i(mn)}} \frac{\partial^2 \mathrm{L_i(mn)}}{\partial mn^2} = \frac{1}{(\rho\psi)_i} [\nabla.\Gamma_i \nabla T_i + P_i] - \upsilon_i.\nabla T \tag{11}$$

$$T_i(t) = \frac{\mathrm{L_i(mn)}}{\Omega \left[(\rho\psi)_i \times \frac{\partial^2 \mathrm{L_i(mn)}}{\partial mn^2} \right]} [\nabla.\Gamma_i \nabla T_i + P_i] - \upsilon_i.\nabla T \tag{12}$$

Fig. 1 shows the proposed paradigm for measuring the effect of patch antenna-brain connectivity on head temperature. To represent the total temperature affecting the head, consider the plan of work in the 3-D spherical coordinate system with a Euclidean metric. The use of Eqs. (2), (6) and (12) is represented in the following Eq. (13):

Then temperature T could be calculated from Eq. (11), and for the sake of simplicity, the following equation is derived:

$$\begin{aligned} T_i(t) = & \frac{\mathrm{L_i(mn)}}{\Omega \left[(\rho\psi)_i \times \frac{\partial^2 \mathrm{L_i(mn)}}{\partial mn^2} \right]} \\ & \left[\begin{array}{l} \frac{1}{r^2} \frac{\partial \left(r^2 \Gamma_i \left(\frac{1}{r^2} \frac{\partial (r^2 T_{ir})}{\partial r} + \frac{1}{r(\sin\theta)} \frac{\partial}{\partial \theta} (T_i(\sin\theta)) + \frac{1}{r(\sin\theta)} \frac{\partial}{\partial \phi} T_i \phi \right)_r \right)}{\partial r} + \\ \frac{1}{r(\sin\theta)} \frac{\partial}{\partial \theta} \left(\Gamma_i \left(\frac{1}{r^2} \frac{\partial (r^2 T_{ir})}{\partial r} + \frac{1}{r(\sin\theta)} \frac{\partial}{\partial \theta} (T_i(\sin\theta)) + \frac{1}{r(\sin\theta)} \frac{\partial}{\partial \phi} T_i \phi \right) (\sin\theta) \right) + \\ \frac{1}{r(\sin\theta)} \frac{\partial}{\partial \phi} \Gamma_i \left(\frac{1}{r^2} \frac{\partial (r^2 T_{ir})}{\partial r} + \frac{1}{r(\sin\theta)} \frac{\partial}{\partial \theta} (T_i(\sin\theta)) + \frac{1}{r(\sin\theta)} \frac{\partial}{\partial \phi} T_i \phi \right) \phi_i + \\ \left(\frac{1}{2\sqrt{\frac{\mu}{\varepsilon}}} \int_0^{2\pi} \int_0^{2\pi} \left(|E_\theta|^2 + |E_\phi|^2 \right) (r^2) (\sin\theta) d\theta d\phi \right)_i \end{array} \right] \\ & - \upsilon_i. \left(\frac{1}{r^2} \frac{\partial (r^2 T_r)}{\partial r} + \frac{1}{r(\sin\theta)} \frac{\partial}{\partial \theta} (T(\sin\theta)) + \frac{1}{r(\sin\theta)} \frac{\partial}{\partial \phi} T \phi \right) \end{aligned} \tag{13}$$

Eq. (13) represents a direct relationship between the properties of the patch antenna material and the degree of the temperature affecting the head.

If Eq. (1) is integrated over the tissue and blood sub-volumes separately, then it can be represented as follows:

$$\int_{vi} \left((\rho\psi)_i \frac{\partial T_i}{\partial t} + \upsilon_i.\nabla T \right) dv = \int_{vi} (\nabla.\Gamma_i \nabla T_i) dv + \int_{vi} P_i dv \tag{14}$$

By solving the integral in Eq. (14), it could be represented as follows:

$$\left((\rho\psi)_i \frac{\partial T_i}{\partial t} + \upsilon_i.\nabla T\right) + C1i = (\nabla.\Gamma_i \nabla T_i) + C2i + P_i + C3i \tag{15}$$

where c1, c2 and c3 are constants of the integral solution. If we consider one constant Ci, where Ci = C2i + C3i-C1i, then Eq. (15) can be represented as follows:

$$\left((\rho\psi)_i \frac{\partial T_i}{\partial t} + \upsilon_i.\nabla T\right) = (\nabla.\Gamma_i \nabla T_i) + P_i + C_i \tag{16}$$

By substituting the value of the power with the value of the radiated power of the patch antenna in Eq. (2), the temperature can then be represented in terms of the patch antenna materials as follows:

$$\begin{aligned} T_i(t) = & \frac{\mathrm{L_i(mn)}}{\Omega\left[(\rho\psi)_i \times \dfrac{\partial^2 \mathrm{L_i(mn)}}{\partial mn^2}\right]} \\ & \left[\begin{array}{l} \dfrac{1}{r^2}\dfrac{\partial\left(r^2\Gamma_i\left(\dfrac{1}{r^2}\dfrac{\partial(r^2T_{ir})}{\partial r} + \dfrac{1}{r(\sin\theta)}\dfrac{\partial}{\partial\theta}(T_i(\sin\theta)) + \dfrac{1}{r(\sin\theta)}\dfrac{\partial}{\partial\phi}T_i\phi\right)_r\right)}{\partial r} + \\ \dfrac{1}{r(\sin\theta)}\dfrac{\partial}{\partial\theta}\left(\Gamma_i\left(\dfrac{1}{r^2}\dfrac{\partial(r^2T_{ir})}{\partial r} + \dfrac{1}{r(\sin\theta)}\dfrac{\partial}{\partial\theta}(T_i(\sin\theta)) + \dfrac{1}{r(\sin\theta)}\dfrac{\partial}{\partial\phi}T_i\phi\right)(\sin\theta)\right) + \\ \dfrac{1}{r(\sin\theta)}\dfrac{\partial}{\partial\phi}\Gamma_i\left(\dfrac{1}{r^2}\dfrac{\partial(r^2T_{ir})}{\partial r} + \dfrac{1}{r(\sin\theta)}\dfrac{\partial}{\partial\theta}(T_i(\sin\theta)) + \dfrac{1}{r(\sin\theta)}\dfrac{\partial}{\partial\phi}T_i\phi\right)\phi + \\ \left(\dfrac{1}{2\sqrt{\dfrac{\mu}{\varepsilon}}}\displaystyle\int_0^{2\pi}\int_0^{2\pi}\left(|E_\theta|^2 + |E_\phi|^2\right)(r^2)(\sin\theta)d\theta d\phi\right)_i + C_i \end{array}\right] \\ & - \upsilon_i.\frac{1}{r^2}\frac{\partial(r^2T_r)}{\partial r} + \frac{1}{r(\sin\theta)}\frac{\partial}{\partial\theta}(T(\sin\theta)) + \frac{1}{r(\sin\theta)}\frac{\partial}{\partial\phi}T\phi \end{aligned} \tag{17}$$

The initial condition specifies the value of T at all values of (mn) at t = 0. This initial condition is usually written as follows:

$$\mathrm{T(mn, 0)} \;=\; \mathrm{T0(mn)} \tag{18}$$

The boundary conditions at (mn) = 0 and (mn) = (mn) max, can be functions of time in general.

We can show that the solution in the equation satisfies the original gradient boundary conditions.

$$\left.\frac{\partial T}{\partial(\mathrm{mn})}\right|_{(\mathrm{mn})=0,t} = \left.\frac{\partial \mathrm{L(mn)}}{\partial(\mathrm{mn})}\right|_{(\mathrm{mn})=0,t} + \left.\frac{\partial \mathrm{G(ab(t))}}{\partial(\mathrm{mn})}\right|_{(\mathrm{mn})=0,t} \tag{19}$$

Consider that L (mn) is a function of (mn) only and G(ab(t)) is a function of time only, and therefore we obtain the following result. Dz satisfies the diffusion equation with zero gradient boundary conditions.

$$\begin{aligned} & \frac{\partial T}{\partial t} - \Omega\frac{\partial^2 T}{\partial(mn)^2} = \frac{\partial(\mathrm{Dz} + L(mn) + G(ab(t)))}{\partial t} - \Omega\frac{\partial^2(\mathrm{Dz} + L(mn) + G(ab(t)))}{\partial(mn)^2} = \frac{\partial \mathrm{Dz}}{\partial t} + \frac{\partial G(ab(t))}{\partial t} \\ & - \Omega\frac{\partial^2 \mathrm{Dz}}{\partial(mn)^2} - \Omega\frac{\partial^2 w}{\partial(mn)^2} = 0 \end{aligned} \tag{20}$$

The above paradigm shows the direct relationship between the materials of the patch antenna and the temperature affecting the head. In the next section, we will further discuss the results of the proposed paradigm and the materials that could be used in patch antenna fabrication to reduce the effect of the resultant temperature on the head. The antenna directivity is calculated from Eq. (21) as follows:

$$D = \frac{4\pi}{\iint P_n(\theta, \varnothing) d\Omega} \tag{21}$$

where P is the power density of the transmitted signal and Ω is the beam area. The equation of the gain of the antenna is dependent on its directivity, where the gain G is calculated as follows:

G = kD. Here, k is the antenna efficiency factor, so we want to decrease the transmitted power to increase the directivity and the gain. Because the coefficient of thermal conductivity λ is defined as the rate of transfer of energy across unit area of surface, when there is a unit temperature gradient, perpendicular to the surface, the rate at which energy is transported is then proportional to the number of carriers of energy and, therefore, to the pressure as well. Then if the thermal material decreases the transferred or transmitted energy, the power will decrease. In our simulation using COMSOL Multiphysics simulation software, we used materials with very low thermal conductivity. The thermal conductivity of lithium niobate was 0.082 W/(m·K); of bismuth telluride, 1.20 W/(m·K); and of casting cast steel, 1.9 W/(m.K).

It is clear that our proposed material will play an important role in increasing the antenna gain and directivity. In the proposed model, materials with poor thermal conductivity were used. There is a clear relationship between the thermal conductivity of the metal from which the antenna is made and the amount of energy, and therefore the power, emitted from it. As the thermal conductivity of the metal increases, the energy from the antenna increase, so our choice of materials would reduce the energy emitted by the antenna. Since the emitted energy is inversely proportional to the antenna gain, it is expected to increase the antenna gain and reduce the amount of energy to which the head is exposed.

3 System Results and Discussions

To validate the model, the proposed structure was simulated in COMSOL Multiphysics software using SAR in the human brain [18]. The human head geometry is a similar geometry given by IEEE, IEC, and CENELEC from their standard particular of SAR esteem estimations. The first geometry underwent minor alterations before being brought into COMSOL Multiphysics. Moreover, the model examples some material parameters with a volumetric introduction work that gauges the variety of tissue type inside the head. The model used the 3D X-ray information to coordinate the type of the imported head geometry in COMSOL Multiphysics. The radiation originates from a fix radio wire set on the left half of the head. The fix receiving wire is energized by a lumped port. The perfusion rate change in various parts of the human body. The interjection work utilized for the electric parameters similarly models the difference in perfusion rate between the tissue inside the head and the skin and bone elsewhere. Because they are the natural temperatures around the head, the temperature values used to analyze the results range from 16.85°C to 36.85°C. We converted the Celsius temperatures to their equivalents in Kelvin because our simulation is based on the Kelvin scale. This temperature range is equivalent to the values 290°K, 295°K, 300°K, 305°K,and 310°K. Fig. 2 shows the head temperature distribution at 290°K using a patch antenna made of traditional materials. The head, in this case, is exposed to a wide distribution of temperatures throughout the whole up to any -2.55×10^{-27} K and can be described as the severely dangerous degree of danger to which the head is exposed. Fig. 3 shows the head temperature distribution at 295°K using a patch antenna made of traditional materials. This case shows that the head is exposed to a wider distribution of more severe temperatures than the previous cases. It reaches its maximum degree in different areas of the head up to -0.26×10^{-26} K and the severity can still be described as severe. Fig. 4 shows the head temperature distribution at 300°K using a patch antenna made of traditional materials.

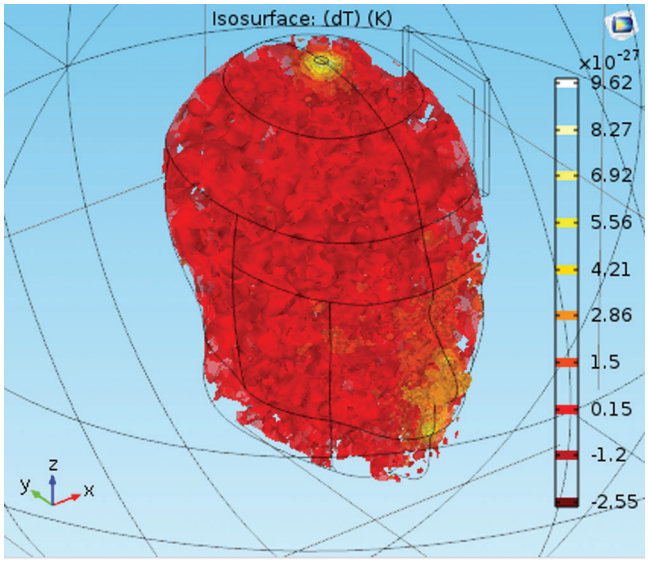

Figure 2: Head temperature distribution at 290°K using patch antenna with its traditional material

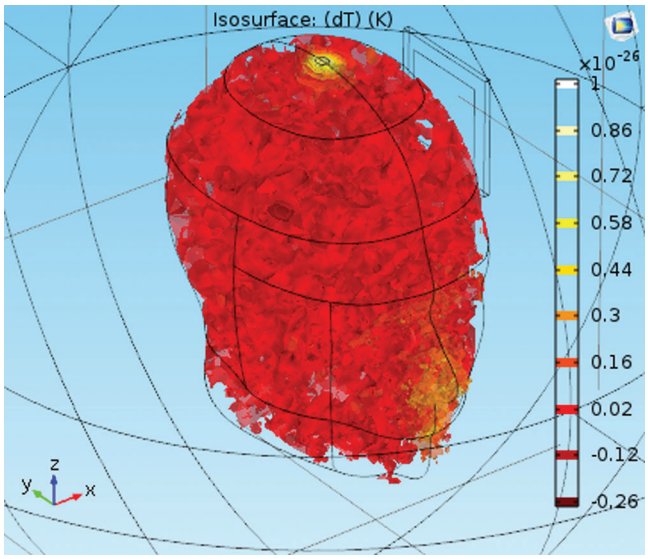

Figure 3: Head temperature distribution at 295°K using patch antenna with its traditional material

However, the temperature distribution is less sharp than in the previous cases. However, the condensed areas are as intense as -0.17×10^{-26} K, but the degree of risk can be described as average. Fig. 5 shows the head temperature distribution at 305°K using a patch antenna made of traditional materials. This case shows that the head is exposed to the lowest temperature distribution of all. Most of the map pear in front of the head and are estimated at -0.22×10^{-26} K but can be described as low risk.

Fig. 6 shows the head temperature distribution at 310°K using a patch antenna made of traditional materials. The temperature distribution in this figure can be characterized by the average as well as the degree of severity, where the maximum value of the temperature is -2.46×10^{-27} K. Fig. 7 shows the head temperature distribution at 290°K using a patch antenna made of casting cast steel. It appears from the figure that the temperature distribution on the head is of medium intensity, and can be described as

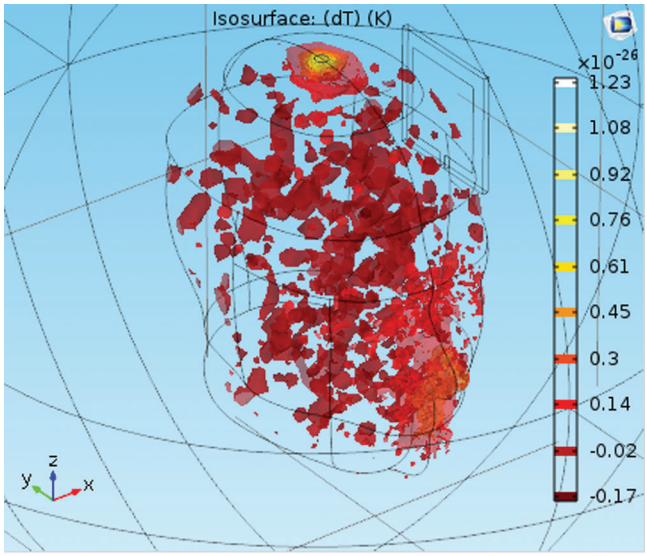

Figure 4: Head temperature distribution at 300°K using patch antenna made of traditional material

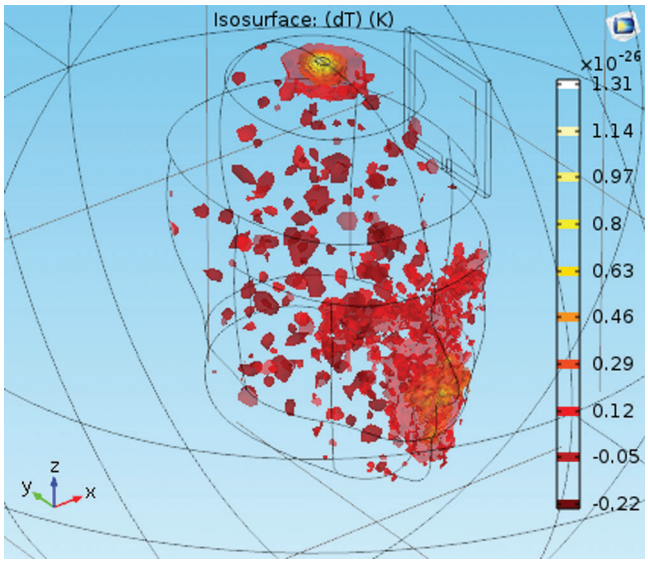

Figure 5: Head temperature distribution at 305°K using patch antenna made of traditional material

average risk, and the maximum temperature distribution in front of the face can reach -0.22×10^{-26} K. Fig. 8 shows the head temperature distribution at 295°K using a patch antenna made of casting cast steel. It appears that the temperature distribution is widespread in all parts of the head and can reach a density up to -2.35×10^{-27} K.This density is concentrated in the area of the face, so it can be said that the degree of severity. Fig. 9 shows the head temperature distribution at 300°K using a patch antenna made of casting cast steel.

It is clear from the figure that the temperature distribution is gradually approaching a high-intensity and high-risk situation due to the concentration of most temperatures in the upper regions of the head at up to -0.17×10^{-26} K. Fig. 10 shows the head temperature distribution at 305°K using a patch antenna made of casting cast steel. Although temperatures are widely distributed in the background of the head, but this

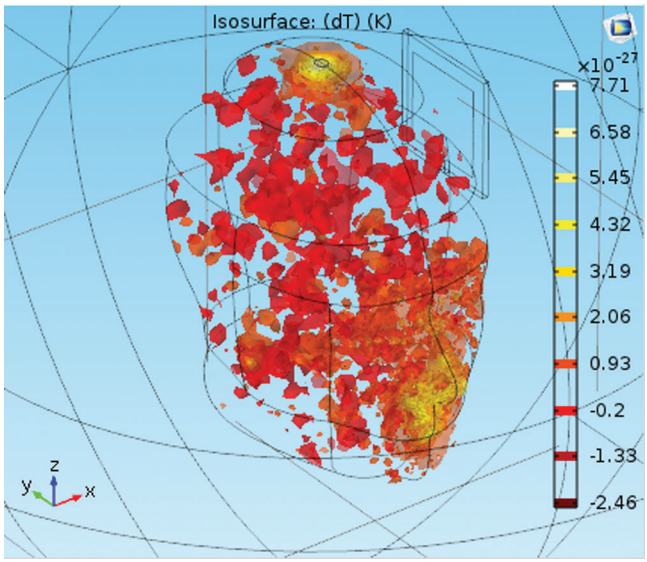

Figure 6: Head temperature distribution at 310°K using patch antenna made of traditional material

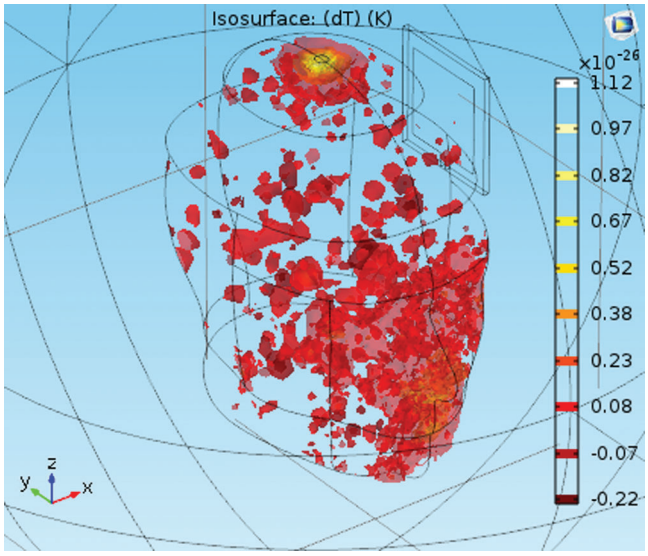

Figure 7: Head temperature distribution at 290°K using patch antenna made of casting cast steel material

condition is very dangerous due to the intensity of temperatures that can reach the maximum at -0.33×10^{-26} K. Fig. 11 shows the head temperature distribution at 310°K using a patch antenna made of casting cast steel. The temperature distribution here is average and the majority of it is in the facial area, with a relatively small intensity up to -2.82×10^{-27} K. The degree of risk can be described as moderate.

Fig. 12 shows the head temperature distribution at 290°K using a patch antenna made of bismuth telluride material. The distribution of the average density of the temperature and the average risk is mostly concentrated in the facial area, and the maximum value of temperature in this case is -0.42×10^{-26} K. Fig. 13 shows the head temperature distribution at 295°K using a patch antenna made of bismuth telluride material. It shows a very dense distribution with an extreme temperature hazard. The density is noticeable in the head background and the temperature reaches -0.28×10^{-26} K. Fig. 14 shows the head

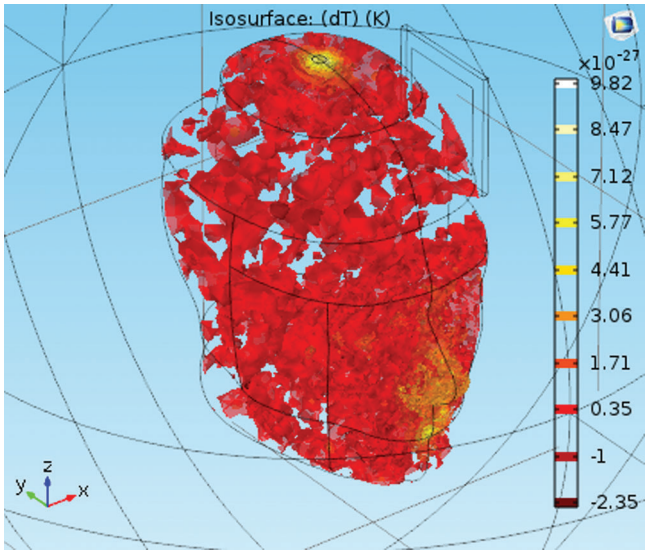

Figure 8: Head temperature distribution at 295K using patch antenna with casting cast steel material

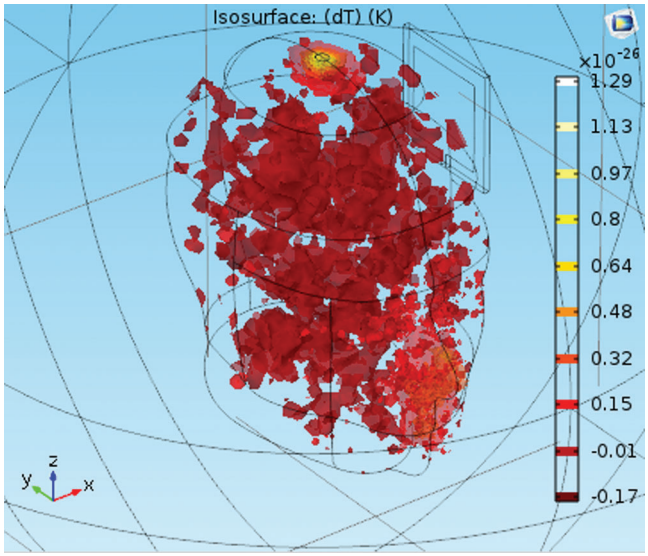

Figure 9: Head temperature distribution at 300K using patch antenna with casting cast steel material

temperature distribution at 300°K using a patch antenna made of bismuth telluride material. Here the danger is severe, due to intensive distribution of temperature in all areas of the head, and the maximum temperature reaching -0.29×10^{-26} K. Fig. 15 shows the head temperature distribution at 305°K using a patch antenna made of bismuth telluride material. This situation is considered more serious than other cases due to the high density of temperature in all areas of the head and a high concentration of up to -0.15×10^{-26} K. Fig. 16 shows the head temperature distribution at 310°K using a patch antenna made of bismuth telluride material. This condition is also very serious, but to a lesser degree than the previous cases. Although the temperature distribution occurs in all areas of the head, the temperature only reaches a maximum of -3.61×10^{-27} K. Fig. 17 shows the head temperature distribution at 290°K using a patch antenna made of barium sodium niobate material. Although the distribution of temperature is not to all areas of the head

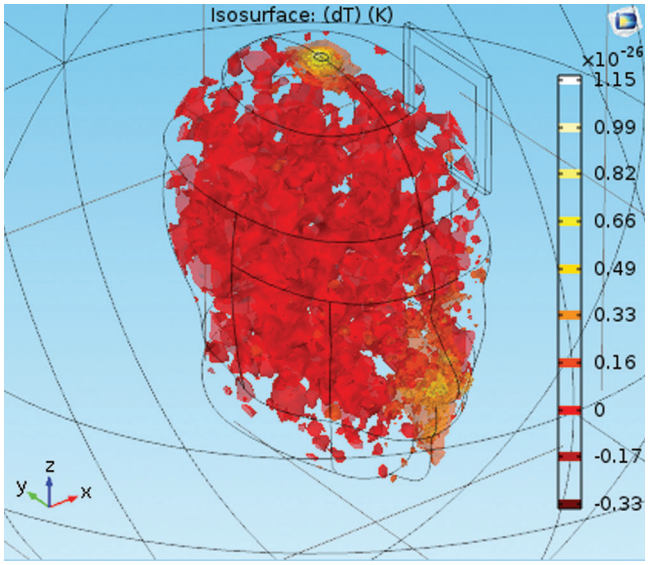

Figure 10: Head temperature distribution at 305°K using patch antenna made of casting cast steel material

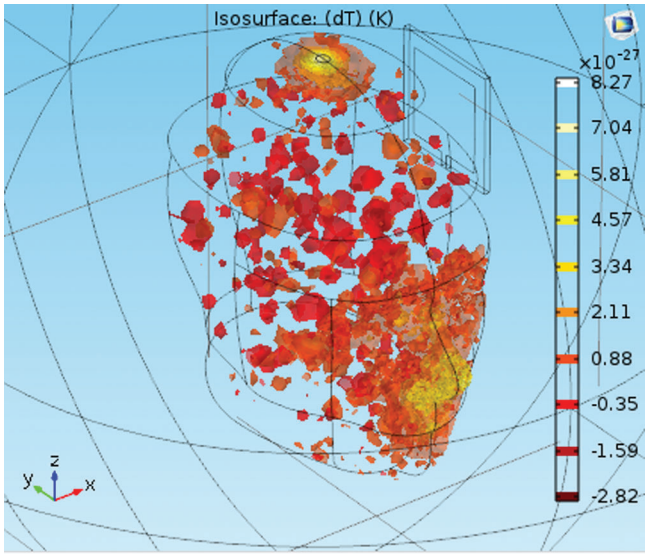

Figure 11: Head temperature distribution at 310°K using patch antenna made of casting cast steel material

with high density, this situation is very serious due to the intensity of temperature in the areas exposed to it, where it reaches -0.31×10^{-26} K. Fig. 18 shows the head temperature distribution at 295°K using a patch antenna made of barium sodium niobate material.

This situation is described as dangerous as the temperature distribution is condensed in all areas of the head and the maximum temperature can reach -0.25×10^{-26} K. Fig. 19 shows the head temperature distribution at 300°K using a patch antenna made of barium sodium niobate material. This condition is described as moderately serious despite the condensation of temperatures on the facial area, and the maximum temperature reaches -1.99×10^{-27} K. Fig. 20 shows the head temperature distribution at 305° K using a patch antenna made of barium sodium niobate material. This is a very serious case where there is little condensation of temperature concentrated in the facial area, and the maximum temperature is

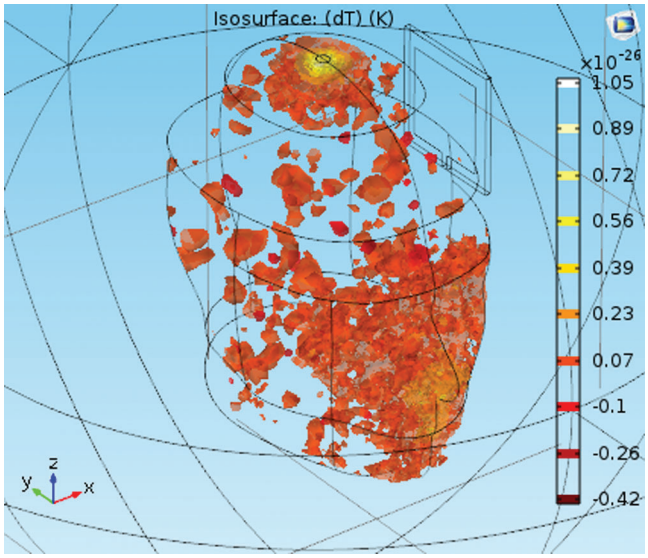

Figure 12: Head temperature distribution at 290°K using patch antenna made ofbismuth telluride material

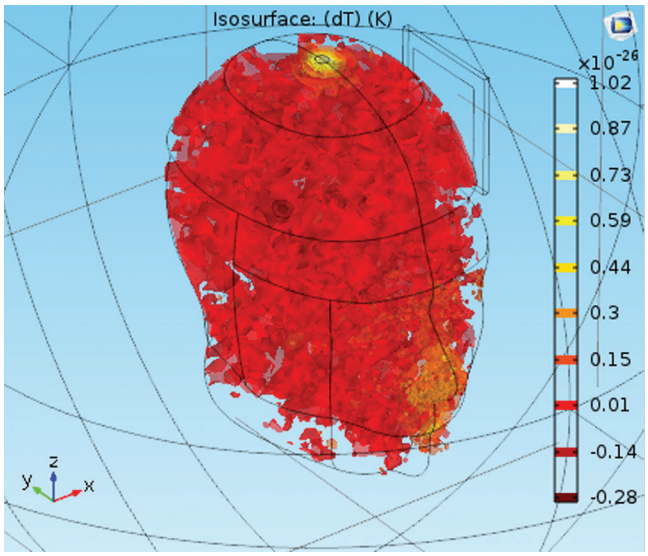

Figure 13: Head temperature distribution at 295°K using patch antenna made ofbismuth telluride material

-0.26×10^{-26} K. Fig. 21 shows the head temperature distribution at 310°K using a patch antenna made of barium sodium niobate material. The degree of risk is moderate due to the low concentration of temperature in the areas of the head except for specific areas of the face, and the maximum temperature is -1.79×10^{-27} K. It is clear from the previous results that the use of any of these materials does not completely eliminate the impact of temperature on the human head, nor the danger to it. However, some materials lower the risk when used in the manufacture of a patch antenna. This effect varies by substance and by temperature. Therefore, this research finds the use of layers of material in the form of thin films covering the outer cover of patch antenna to be mobile and track their movements appearing and concealment movements per film. This is done by using a temperature sensor; when the external temperature is within a specific range, the patch antenna should be covered with a material suitable for that temperature. The material's properties at this temperature can reduce the power of the radiation

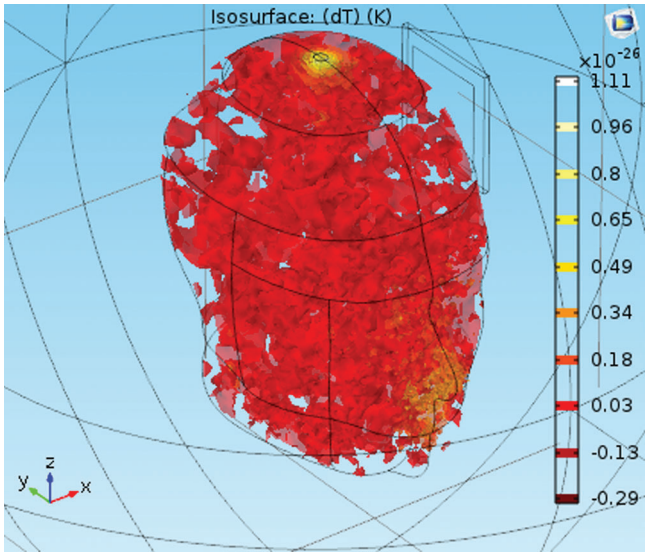

Figure 14: Head temperature distribution at 300K using patch antenna with Bismuth Telluride-Bi2Te3 material

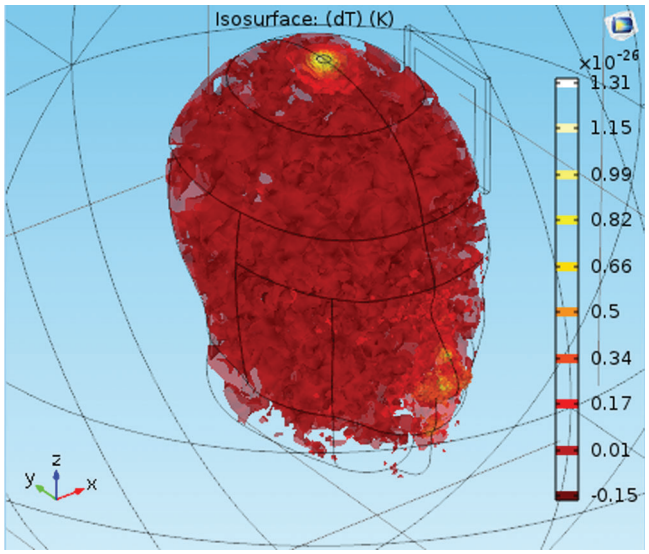

Figure 15: Head temperature distribution at 305K using patch antenna with Bismuth Telluride-Bi2Te3 material

emitted by the antenna, and therefore reduce the temperature on the head. The above results show that it is possible to rely on four types of materials in the manufacture of patch antennas. The traditional material works only at 305°K; casting cast steel work at around 295°K; bismuth telluride works at 290°K; and barium sodium niobate works at around 310°K. The temperature range of 290°K to 310°K has been determined to be the most common range when smartphones are being used. This reduces the head temperature and reduces the risk from high to moderate.

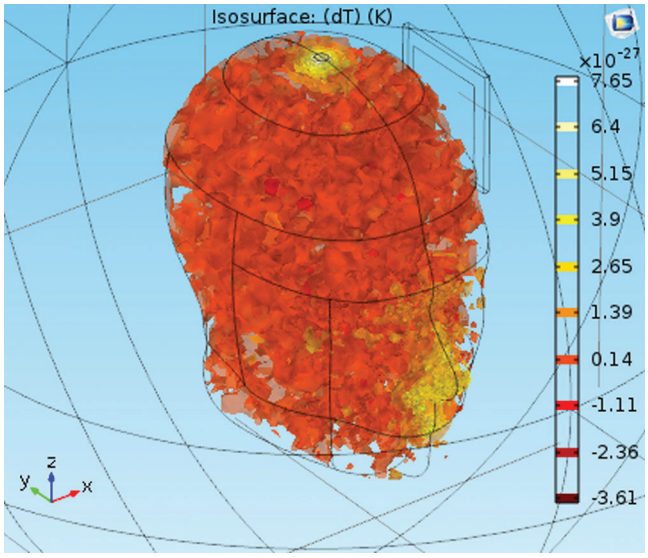

Figure 16: Head temperature distribution at 310°K using patch antenna made of bismuth telluride material

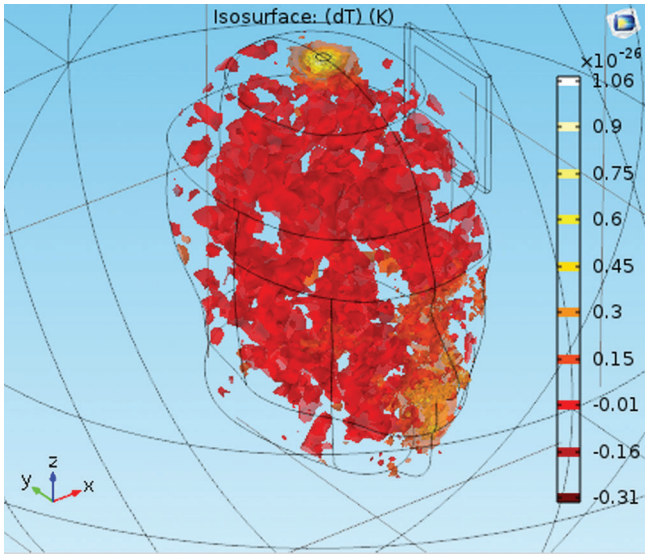

Figure 17: Head temperature distribution at 290°K using patch antenna made of barium sodium niobate material

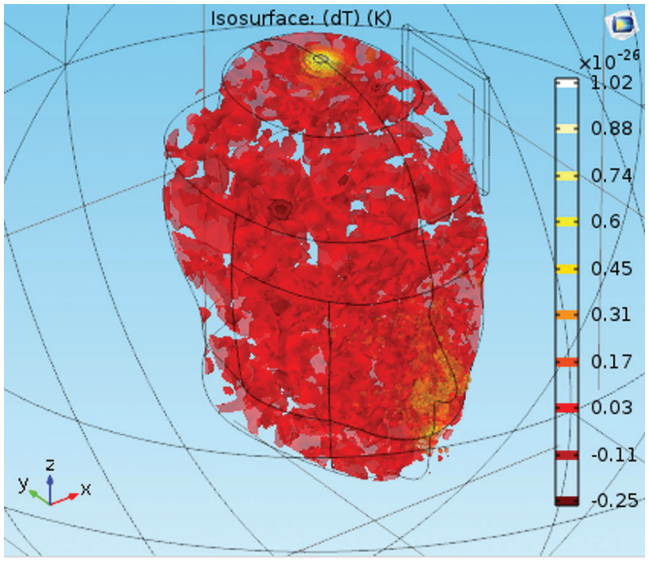

Figure 18: Head temperature distribution at 295°K using patch antenna made ofbarium sodium niobate material

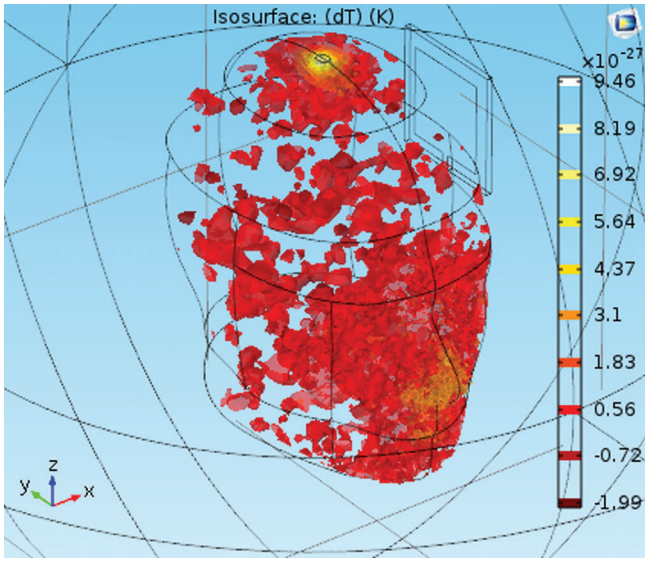

Figure 19: Head temperature distribution at 300°K using patch antenna made ofbarium sodium niobate material

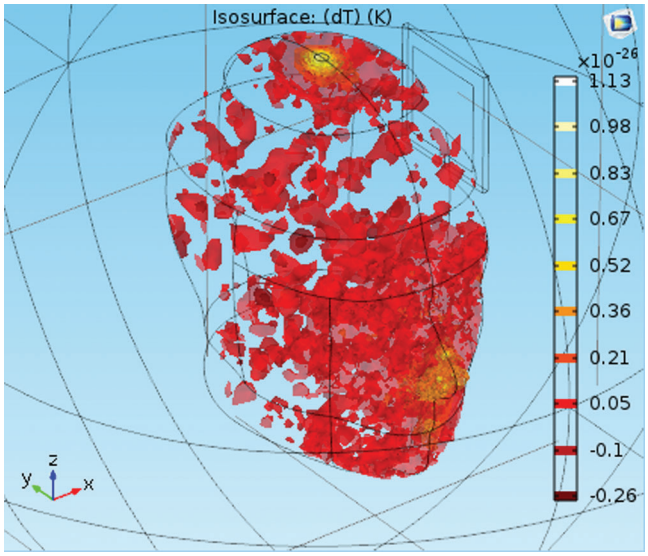

Figure 20: Head temperature distribution at 305°K using patch antenna made of barium sodium niobate material

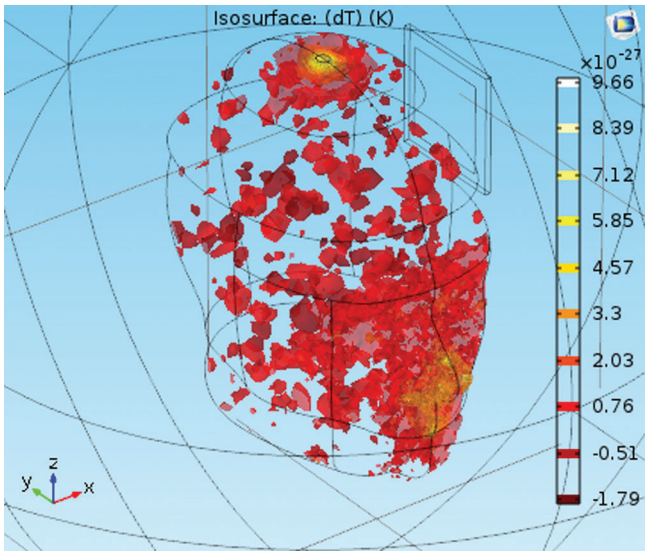

Figure 21: Head temperature distribution at 310°K using patch antenna made of barium sodium niobate material

4 Conclusion

The patch antenna commonly used in poses a risk to human health by creating increased temperature in a person's head. This rise in temperature can adversely affect brain function. The research in this paper presents a new model of virtual communication between the brain and the patch antenna. This model works according to a number of inputs, including blood and tissue, as well as the emission energy of the antenna, which is a function of the characteristics of the metal from which the antenna is made. This model is able to accurately describe the temperature affecting the human head in terms of those inputs. The research then provided a solution, based on this model, to reduce temperatures by covering the patch antenna with one of a number of animated thin films, the choice of which depends on the ambient temperature. Each metal has specific characteristics when exposed to different temperatures that in turn affect the radiation forces

emitted from it. The best results were obtained from four materials: the conventional material of patch antenna, casting cast steel, bismuth telluride (Bi_2Te_3), and barium sodium niobate, which work around temperatures of 305°K, 295°K, 290°K, and 310°K, respectively. Using these metals in this range of temperatures keeps the temperature inside an individual's head as low as possible.

Acknowledgement: The authors extend their appreciation to the Deanship of Scientific Research at King Khalid University for funding this work through Research Groups Program under grant number (R.G.P.2/35/40).

Funding Statement: This research was funded by King Khalid University—KSA, grant number (R.G.P.2/35/40) and the APC was funded by King Khalid University—KSA.

Conflicts of Interest: The authors declare that they have no conflicts of interest to report regarding the present study.

References

1. Stanković, V., Jovanović, D., Krstić, D., Marković, V., Cvetković, N. (2017). Temperature distribution and specific absorption rate inside a child's head. *International Journal of Heat and Mass Transfer, 104,* 559–565. DOI 10.1016/j.ijheatmasstransfer.2016.08.094.
2. Forouharmajd, F., Ebrahimi, H., Pourabdian, S. (2018). Mobile phone distance from head and temperature changes of radio frequency waves on brain tissue. *International Journal of Preventive Medicine, 9,* 61. DOI 10.4103/ijpvm.IJPVM_70_17.
3. Fiser, O., Merunka, I., Vrba, J. (2017). Microwave hyperthermia system for head and neck area with noninvasive UWB temperature change detection. *Progress in Electromagnetics Research Symposium—Spring (PIERS),* pp. 1657–1662.
4. Kaburcuk, F., Elsherbeni, A. Z., Messaoudi, H., Aguili, T., Abushakra, F. Z. et al. (2018). Temperature rise and SAR distribution at wide range of frequencies in a human head due to an antenna radiation. *Applied Computational Electromagnetics Society Journal, 33(4),* 367–372.
5. He, W., Xu, B., Gustafsson, M., Ying, Z., He, S. (2018). RF compliance study of temperature elevation in human head model around 28 GHz for 5G user equipment application: simulation analysis. *IEEE Access, 6,* 830–838. DOI 10.1109/ACCESS.2017.2776145.
6. Mündel, T., Raman, A., Schlader, Z. J. (2016). Head temperature modulates thermal behavior in the cold in humans. *Temperature, 3(2),* 298–306. DOI 10.1080/23328940.2016.1156214.
7. Takagi, Y., Honma, S., Wakamatsu, H., Ito, M. (2015). Comparison of brain temperature distribution in mathematical and solid models of head thermal characteristics. *Electrical Engineering in Japan, 193(2),* 58–68. DOI 10.1002/eej.22642.
8. Makhlouf, O., Cueille, M., Dubard, J. L. (2016). TLM computation of temperature distribution in human head exposed to electromagnetic waves, *IEEE International Symposium on Antennas and Propagation (APSURSI),* pp. 637–638.
9. Hirata, A., Ohta, S., Laakso, I., Fujiwara, O. (2014). Relationship between spatial-averaged SAR and temperature elevation in human head models from 1–10 GHz, *International Symposium on Electromagnetic Compatibility, Tokyo,* pp. 174–177.
10. Wessapan, T., Srisawatdhisukul, S., Rattanadecho, P. (2012). Specific absorption rate and temperature distributions in human head subjected to mobile phone radiation at different frequencies. *International Journal of Heat and Mass Transfer, 55(1–3),* 347–359. DOI 10.1016/j.ijheatmasstransfer.2011.09.027.
11. Wang, Y., Zhang, Y., Liu, X., Wang, J., Wei, L. et al. (2014). Effect of a hydrophilic head group on krafft temperature, surface activities and rheological behaviors of erucyl amidobetaines. *Journal of Surfactants and Detergents, 17(2),* 295–301. DOI 10.1007/s11743-013-1496-7.

12. Thotahewa, K. M., Redoute, J., Yuce, M. R. (2013). SAR, SA, and temperature variation in the human head caused by IR-UWB implants operating at 4 GHz. *IEEE Transactions on Microwave Theory and Techniques, 61(5),* 2161–2169. DOI 10.1109/TMTT.2013.2250515.
13. Chen, C., Fu, S., Norikazu, M., Yang, Y., Liu, Y. et al. (2015). Comparative miRNAs analysis of two contrasting broccoli inbred lines with divergent head-forming capacity under temperature stress. *BMC Genomics, 16(Suppl 12),* 1–19. DOI 10.1186/1471-2164-16-S12-S1.
14. Bhat, M. A., Kumar, V. (2013). Calculation of SAR and measurement of temperature change of human head due to the mobile phone waves at frequencies 900 MHz and 1800 MHz. *Advances in Physics Theories and Applications, 16,* 54–63.
15. Kays, W. M., Whitelaw, J. H. (1966). Convective heat and mass transfer. *Journal of Applied Mechanics, 34(1),* 254.
16. Shrivastava, D., Vaughan, J. T. (2009). A generic bioheat transfer thermal model for a perfused tissue. *Journal of Biomechanical Engineering, 131(7),* 809. DOI 10.1115/1.3127260.
17. Elrashidi, A., Elleithy, K. M., Bajwa, H. (2012). Resonance frequency, gain, efficiency and quality factor of a microstrip printed antenna as a function of curvature for TM 01 mode using different substrates. *Journal of Wireless Networking and Communications, 1(1),* 1–8. DOI 10.5923/j.jwnc.20110101.01.
18. Specific Absorption Rate (SAR) in the Human Brain. (2019). *Available at: https://www.comsol.com/model/specific-absorption-rate-sar-and-temperature-study-in-the-human-brain-2190*.